A Combined Complete Pore Blocking and Cake Filtration Model for Steady-State Electric Field-Assisted Ultrafiltration

Biswajit Sarkar and Sirshendu De
University School of Chemical Technology, GGS Indraprastha University, Delhi 110075, India

Dept. of Chemical Engineering, Indian Institute of Technology, Kharagpur 721 302, India

DOI 10.1002/aic.12667
Published online May 23, 2011 in Wiley Online Library (wileyonlinelibrary.com).

An analysis for the flux decline and identification of dominant fouling mechanism in electric field enhanced cross-flow ultrafiltration (UF) is proposed. The model is developed based on the modification of Hérmia's approach for constant pressure dead-end filtration laws. Electric field-assisted cross-flow UF experiments of synthetic juice (a mixture of pectin and sucrose) are performed in a rectangular flow channel. Using the flux decline data, the dominant fouling mechanism is identified by estimation of model parameters. The effect of various operating conditions such as electric field, feed solute concentration, cross-flow velocity, and transmembrane pressure on the flux decline and the corresponding fouling mechanism are studied. Experimental results show that electric field has significant effect on the onset of cake formation as well as on the enhancement in permeate flux. Model-predicted results are successfully compared with the experimental data. © 2011 American Institute of Chemical Engineers *AIChE J,* 58: 1435–1446, 2012

Keywords: ultrafiltration, electrophoresis, complete pore blocking, cake formation, pectin

Introduction

Application of ultrafiltration (UF) is common for the clarification of fruit and vegetable juices.[1–3] The major restriction in the performance of UF is the decline in permeate flux, which is caused by the concentration polarization and membrane fouling during the operation.[4] Concentration polarization refers to the accumulation of solute within a thin boundary layer adjacent to the membrane surface. Fouling can be irreversible with solute adsorption on or in the membrane pore walls, leading to complete or partial pore blocking. The problem of membrane fouling is particularly significant in UF of fruit juice. Fouling by fruit juice is attributed to the deposition of macromolecular or colloidal species (such as pectin, cellulose, hemicelluloses, tannins, and proteins) on the membrane surface or inside the pores.[5] The extent and nature of transient flux decline depend on the nature and magnitude of the membrane, that is, solute interaction, size and shape of solute, pore size distribution of membrane, and the operating conditions. Various flux decline mechanisms are available in the literature. Some of these are osmotic pressure controlled,[6] cake or gel layer governed,[7,8] and pore blocking controlled.[9,10] Hermans and Bredee[11] have proposed four different kinds of pore-blocking laws, namely, complete blocking, intermediate blocking, standard blocking, and cake layer formation. Hérmia[9] has revised all blocking laws and reformulated the four laws in a common frame for

Correspondence concerning this article should be addressed to S. De at sde@che.iitkgp.ernet.in.

constant pressure dead-end filtration of power-law non-Newtonian fluids. These laws can be extended to Newtonian fluids when the power law index is substituted by 1. In their work, they have used the properties of slurry rather than the cake properties. However, to investigate the fouling mechanism, Hérmia's model has been successfully used by several researchers during dead-end filtration as well as cross-flow UF for a wide range of materials. This includes the separation of various cake-forming solutes such as polymethyl methacrylate,[12] humic acid,[13] and polyethylene glycol.[14] This model has also been used to study the flux decline mechanism for nanofiltration and reverse osmosis of leather plant effluent.[15]

The flux decline data are usually described by only one of these mechanisms[12,16] or sometimes more than one mechanism in succession.[13,17] In most of the studies, it is proposed that the initial rapid flux decline arises from the pore blocking by the physical deposition of the solutes on the membrane surface followed by the cake formation leading to slow flux decline. Ho and Zydney[17] have developed a combined pore blocking and cake filtration model to analyze the flux decline during the stirred batch microfiltration of bovine serum albumin (BSA) solution using polycarbonate track-etched membrane. Yuan et al.[13] have described the flux decline behavior during dead-end microfiltration of humic acid using the model developed by Ho and Zydney.[17]

In cross-flow filtration, membrane fouling is strongly affected by the tangential flow. Therefore, Hérmia's classical constant pressure blocking filtration laws, which are developed for batch system, are incapable to explain the effect of tangential flow on membrane fouling during cross-flow filtration. Nevertheless, there are reports available in the literature those use Hérmia's model for dead-end filtration for analyzing the experimental results in cross-flow filtration. These are filtration of BSA solution,[18] activated sludge wastewater,[19] colloidal suspension of bentonite in the presence of macromolecules,[20] and polyethylene glycol.[14] Field et al.[10] have introduced the effects of cross-flow removal mechanism into the Harmia's approach for the first time and derived the governing equations of various blocking laws for cross-flow filtration. Giorno et al.[21] have investigated the effect of enzyme on the membrane fouling and permeate flux during cross-flow UF of apple juice. They have observed that in the absence of the enzyme, the flux decline is governed by a cake filtration mechanism, whereas in the presence of the enzyme, the prevailing fouling mechanism is complete pore blocking. Todisco et al.[1] have used a modified set of equations that are developed for classical dead-end filtration to identify the fouling mechanism during cross-flow microfiltration of orange juice. The results show that separation process is controlled by cake filtration mechanism at relatively low cross-flow velocity and at low pressure. At higher cross-flow velocity and higher pressure, filtration is controlled by a complete pore-blocking mechanism. Barros et al.[22] have examined the fouling mechanism of cross-flow UF of depectinized pineapple juice on both ceramic tubular membrane and polysulfone hollow fiber membrane using the model developed by Field et al.[10] Their analyses revealed that cake filtration mechanism prevails in hollow fiber and that complete pore-blocking mechanism is dominant in ceramic tubular membrane. Rai et al.[23] have studied the cross-flow UF of depectinized mosambi juice. Recently, Mondal and De[24] have developed a generalized model considering sequential presence of complete pore blocking and cake filtration mechanism for a continuous steady cross-flow filtration.

Application of external direct current (d.c.) electric field with appropriate polarity across the membrane surface shows potential to reduce the membrane fouling and concentration polarization in case of filtration of charged particles.[25,26] In electro-UF, electric field (acts as an additional driving force to the transmembrane pressure) imposes an electrophoretic force on charged particles that drag them away from the membrane surface. Therefore, the concentration polarization and membrane fouling are reduced resulting in an enhancement of permeate flux. To design and scale up the electro-UF system, the flux decline mechanism should be properly understood. Iritani et al.[27] have developed a mathematical model to describe the permeate flux decline in inclined and downward electro-UF of protein (BSA) solution. In our earlier work,[28–30] we developed a model based on gel layer theory to quantify the flux decline with time during cross-flow electro-UF of synthetic juice (mixture of sucrose and pectin) and mosambi juice. In that model, the membrane fouling due to pore blocking and adsorption on the membrane pore walls were not considered. There is currently no theoretical analysis available in the literature for identification of fouling mechanism and quantification of flux decline in electric field-assisted cross-flow UF. Therefore, it is warranted to develop pertinent model equations under a general framework for identification of fouling mechanism and quantification of flux decline for continuous cross-flow electric field-assisted UF. In the current work, a model is developed by modifying Hérmia's approach[9] and the theory proposed by Field et al.[10] to depict for the cross-flow filtration. Sequential occurrence of complete pore blocking and cake filtration mechanisms is considered to account the transient flux decline behavior during electric field-assisted cross-flow filtration. To the authors' knowledge, in case of electric field-enhanced UF, this model is first of its kind. The model is tested using experimental data for filtration of synthetic juice over a wide range of operating conditions.

Theory

Modification of Hérmia's formulation for complete pore-blocking case in the presence of electric field during an unstirred batch filtration

In this model, the membrane fouling is assumed to be started with complete pore blocking, i.e., solutes arriving to the membrane surface due to convective force, block some of the pore entrance without any superimposition. This leads to decrease in membrane surface available for filtration. In the presence of electric field, the probability of pore blocking is reduced due to electrophoresis. Hence, in the presence of external d.c. electric field, the governing equation of flux decline due to pore blocking can be written from modified Hérmia's model as[9]

$$\frac{dJ}{dt} = -k_b(J - J_e) \tag{1}$$

where J_e is the electrophoretic velocity[31] ($J_e = \frac{\varepsilon_0 D_i \xi}{\eta} E$). The solution of Eq. 1 results in the following expression

$$J = (J_0 - J_e)\exp(-k_b t) + J_e \quad (2)$$

where J_0 is the initial permeate flux ($\Delta P/\mu\, R_m$).

In terms of resistance, the expression of permeate flux is written as

$$J = \frac{J_0}{1 + R^*_{CPB}} \quad (3)$$

where R^*_{CPB} is the dimensionless complete pore-blocking resistance, which can be written in terms of complete pore-blocking resistance (R_{CPB}) and hydraulic membrane resistance (R_m) as $R^*_{CPB} = \frac{R_{CPB}}{R_m}$.

From Eqs. 2 and 3, the expression of complete pore-blocking resistance is obtained

$$R^*_{CPB} = \frac{\exp(\tau) - A_1 - A_4\exp(\tau)}{A_1 + A_4\exp(\tau)} \quad (4)$$

where $\tau = k_b t$, $A_1 = \frac{J_0 - J_e}{J_0}$, $A_4 = \frac{J_e}{J_0}$.

In case of cross-flow filtration, it is assumed that complete pore blocking prevails initially up to a time t_1 followed by the growth of cake layer over the membrane surface. The thickness of the cake layer is restricted by the forced convection imposed by the cross flow of the retentate.

Flux decline for $t \le t_1$

In continuation of the discussion presented in the preceding section, assuming only one blocking mechanism, i.e., complete pore blocking occurs up to $t \le t_1$, the permeate flux is therefore expressed as

$$J = (J_0 - J_e)\exp(-\tau) + J_e \quad (5)$$

Flux decline for $t > t_1$

It is assumed that formation and growth of cake layer occur after pores are completely blocked and that the growth of cake layer is restricted due to the presence of external cross-flow velocity of feed and d.c. electric field. Thus, only cake filtration mechanism prevails beyond $t > t_1$, and the corresponding flux decline equation is modified from that proposed by Field et al.[10]

$$\frac{dJ}{dt} = -k_c J^2 \left[J - J'_s\right] \quad (6)$$

where $J'_s (J'_s = J_s + J_e)$ is the steady-state permeate flux in the presence of electric field. J_s is the steady-state flux at zero electric field.

The permeate flux can be written in terms of resistance as

$$J = \frac{\Delta P}{\mu\left[R_m + R_{CPB}(t_1) + R_c(t - t_1)\right]} \quad (7)$$

or

$$J = \frac{J_{t_1}}{1 + R^{**}_c} \quad (8)$$

where $R^*_c = \frac{R_c}{R_m}$, $R^{**}_c = \frac{R^*_c}{1 + R^*_{CPB}}$, and $J_{t_1} = \frac{J_0}{1 + R^*_{CPB}}$.

Taking the derivative of Eq. 8 with respect to t, the rate of change of flux is obtained as

$$\frac{dJ}{dt} = -\frac{J_{t_1}}{(1 + R^{**}_c)^2}\frac{dR^{**}_c}{dt} \quad (9)$$

Equating Eqs. 6 and 9 and using Eq. 8, the governing equation of the cake layer resistance is obtained

$$\frac{dR^{**}_c}{dt} = \frac{k_c J_{t_1}}{(1 + R^{**}_c)}\left[J_{t_1} - J'_s(1 + R^{**}_c)\right] \quad (10)$$

Equation 10 can be solved with the initial condition, i.e., at $t = t_1$, $R^*_c = 0$ and the solution becomes

$$R^{**}_c + \frac{J_{t_1}}{J'_s}\ln\frac{J_{t_1} - J'_s(1 + R^{**}_c)}{J_{t_1} - J'_s} = -k_c J_{t_1} J'_s (t - t_1) \quad (11)$$

Conditions for continuity of flux

It is assumed that the flux values as well as time derivatives of flux are continuous at time t_1, as both the pore blocking and cake formation coincides at time t_1. It may be observed from Eqs. 5 and 7 that the flux values are continuous at $t = t_1$. The continuity of slope of J vs. t at $t = t_1$ is obtained as follows

$$\left.\frac{dJ}{dt}\right|_{t=t-\delta} = \left.\frac{dJ}{dt}\right|_{t=t+\delta} \quad (12)$$

At $t = t_1$ and $\delta \to 0$ in the regime $t \le t_1$, the following equation is obtained from Eq. 2

$$\left.\frac{dJ}{dt}\right|_{t=t_1} = -k_b(J_0 - J_e)\exp(-\tau_1) \quad (13)$$

At $t = t_1$ and $\delta \to 0$ in the regime $t \ge t_1$, the following equation is obtained from Eq. 6

$$\left.\frac{dJ}{dt}\right|_{t=t_1} = -k_c J^2_{t_1}(J_{t_1} - J'_s) \quad (14)$$

where $J_{t_1} = (J_0 - J_e)\exp(-\tau_1) + J_e$.

Equating Eqs. 13 and 14 and using the fact that $J'_s = J_s + J_e$, the following expression is obtained

$$\frac{(J_0 - J_e)k_b}{\exp(\tau)_1} = k_c[(J_0 - J_e)\exp(-\tau_1) + J_e]^2[(J_0 - J_e) \times \exp(-\tau_1) - J_s] \quad (15)$$

Equation 15 can be rearranged as

$$\left[\exp(\tau_1)\right]^3 + a_1\left[\exp(\tau_1)\right]^2 + a_2\left[\exp(\tau_1)\right] + a_3 = 0 \quad (16)$$

where

$a_1 = \left(\frac{J_0}{J_s} - \frac{J_e}{J_0}\right)\left(\frac{1}{A_3} - 1\right) - 2\left(1 - \frac{J_0}{J_e}\right)$;

$a_2 = \left(1 - 2\frac{J_e}{J_s}\right)\left(1 + \frac{J_0^2}{J_e^2}\right) - 4\frac{J_0}{J_s}$;

$a_3 = \frac{J_e}{J_s} - \frac{J_0}{J_s}\left(\frac{J_0^2}{J_e^2} - 3\frac{J_0}{J_s} - 3\right)$ and $A_3 = \frac{k_c J_e^2}{k_b}$

As $Q^3 + R^2 < 0$, where $Q = \frac{3a_2 - a_1^2}{9}$; $R = \frac{9a_1a_2 - 27a_3 - 2a_1^3}{54}$, the solution of Eq. 16 becomes[32]

$$\exp(\tau_1) = \left[2\sqrt{-Q}\cos\left(\frac{\theta}{3}\right) - \frac{a_1}{3}\right] \tag{17a}$$

where $\cos\,\theta = R/\sqrt{-Q^3}$. The other two roots are complex and hence neglected. Thus, the expression of τ_1 becomes

$$\tau_1 = \ln\left[2\sqrt{-Q}\cos\left(\frac{\theta}{3}\right) - \frac{a_1}{3}\right] \tag{17b}$$

Conditions for various domains

At steady state, $\frac{dR_c^{**}}{dt} = 0$, the following expression is resulted from Eq. 10

$$J_{t_1} = J_s'(1 + R_{cs}^{**}) \tag{18}$$

Using the definition of R_{cs}^{**}, Eqs. 8, and 18, R_{cs}^{**} can be expressed in terms of initial and steady-state flux

$$\frac{R_{cs}^{*}}{R_{CPB}^{*}} = \frac{R_{cs}}{R_{CPB}} = \frac{1}{R_{CPB}^{*}}\left(\frac{J_0}{J_s'} - 1\right) - 1 \tag{19}$$

Using Eqs. 4 and 19, the conditions for various fouling domains are quantified as described later. The condition for infeasible solution $\left(\frac{R_{cs}^{*}}{R_{CPB}^{*}} = \frac{R_{cs}}{R_{CPB}} < 0\right)$ is as follows

$$\frac{J_s'}{J_0} > \frac{1 - A_4\left[(1 - \exp(\tau_1)\right]}{\exp(\tau_1)} \tag{20}$$

The condition for pore-blocking dominating region is

$$\frac{J_s'}{J_0} > \frac{1 - A_4\left[(1 - \exp(\tau_1)\right]}{1.5\,\exp(\tau_1) - 0.5\left[1 - A_4(1 - \exp(\tau_1)\right]} \tag{21}$$

For cake formation dominating region, $\left(\frac{R_{cs}^{*}}{R_{CPB}^{*}} = \frac{R_{cs}}{R_{CPB}} > 1.5\right)$ is

$$\frac{J_s'}{J_0} < \frac{1 - A_4\left[(1 - \exp(\tau_1)\right]}{2.5\,\exp(\tau_1) - 1.5\left[1 - A_4(1 - \exp(\tau_1)\right]} \tag{22}$$

Estimation of primary model parameters (k_b and k_c) and identification of fouling mechanism

1. From the knowledge of membrane permeability and operating transmembrane pressure, pure water flux (J_0) is calculated. For a particular value of electric field, electrophoretic velocity (J_e) is estimated for a given feed solution (viscosity and zeta potential values are known). From the experimental flux decline data, the value of steady-state flux, J_s' is obtained. Knowing the value of J_e, the steady-state flux without electric field (J_s) can be calculated by its definition as $J_s = J_s' - J_e$. Next, the values of k_b and k_c are guessed. Hence, τ is calculated from Eq. 17. After that, the complete pore-blocking time t_1 is calculated from its definition $\tau = k_b t_1$.

2. For $t < t_1$, permeate flux values at various operating time are calculated using Eq. 5.

3. For $t > t_1$, first, Eq. 11 is solved iteratively using Newton-Raphson technique at every time point, and the corresponding permeate flux value is calculated using Eq. 8.

4. Now, for the entire duration of filtration, at corresponding operating time, the sum of errors between calculated and experimental flux values are computed using an optimization algorithm (Direct search algorithm of IMSL MATH library) as $S = \sum_{i=1}^{n}\left(\frac{J_{i,exp} - J_{i,cal}}{J_{i,exp}}\right)^2$, where $J_{i,exp}$ is the experimental flux and $J_{i,cal}$ is the calculated flux at ith operating time.

5. If S is less than 0.001, the program is terminated and the transient profile of permeate flux is obtained. The corresponding values of k_b and k_c are recorded. If not, another set of values of k_b and k_c is guessed in Step (1), and the process is continued till the given convergence is achieved.

6. With the estimated values of k_b and k_c and with the knowledge of $\frac{J_s'}{J_0}$ and $\frac{J_e'}{J_0}$, one can estimate the value of complete pore blocking time, τ_1 from Eq. 17. Knowing the three parameters, $\frac{J_s'}{J_0}$, $\frac{J_e}{J_0}$, and τ_1, various domains of fouling can be computed using Eqs. 20–22 as shown in Figures 1 and 2.

Materials and Methods

Materials

Flat-sheet polyethersulfone membrane of molecular weight cutoff 50 kDa, procured from M/s, Permionics (Boroda, India), was used for UF of synthetic juice (a mixture of pectin and sucrose). Pure pectin (average molecular weight 65 kDa; supplied by Loba-Chemie, India) and pure sucrose (obtained from Merck, India) were used for the experiments. The hydraulic resistance of the membrane was determined using distilled water, and it was estimated as $13.1 \times 10^{12}\ m^{-1}$.

Electro-UF cell

The schematic of electro-UF cell was shown elsewhere.[28] A brief discussion of this setup is presented here. The feed solution was pumped from a 10-L feed tank and was allowed to flow tangentially over the membrane surface through a thin rectangular channel (length: 37 cm; width: 3.6 cm; and height: 6.5 mm). The membrane was placed on a porous stainless steel plate, which acted as a cathode. A platinum-coated titanium sheet (length: 33.5 cm; width: 3.4 cm; and thickness: 1.0 mm) was used as the anode and was positioned parallel to the flow position just above the flow channel. These two electrodes were connected with the externally regulated d.c. power supply by stainless steel connectors from which electric field was applied across the membrane surface. The transmembrane pressure and the flow rate were maintained by adjusting the retentate and bypass valve. The flow rate was measured by a rotameter placed on the outlet of the cell, and the pressure was measured by a pressure gauge. The permeate was collected from the bottom of the cell, and the retentate was returned back to the feed tank. The effective area of the membrane was 133.2 cm^2.

Operating conditions

Electro-UF experiments were designed to observe the influence of operating conditions (i.e., electric field, cross-flow velocity, transmembrane pressure, and feed concentration) on the steady state as well as transient permeate flux. The feed solution for the experiments was prepared by

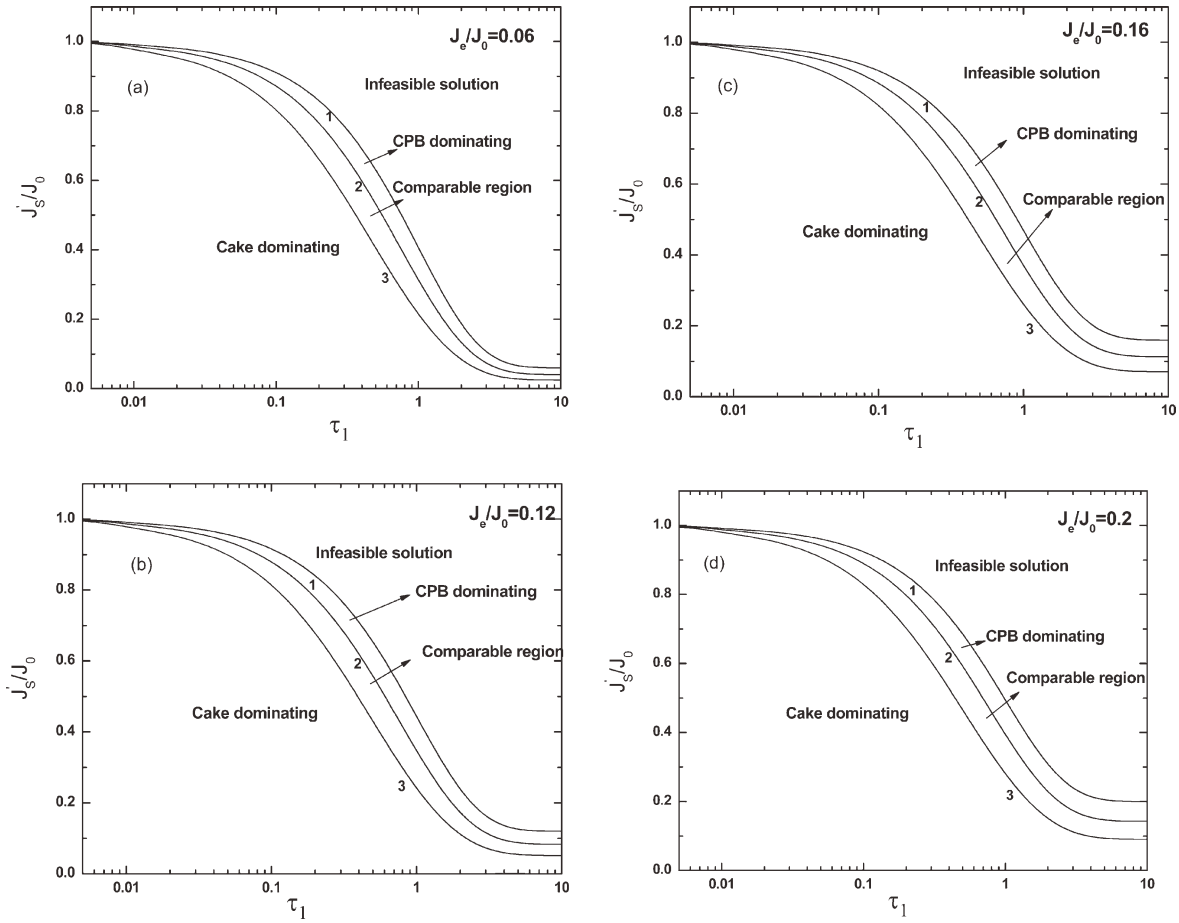

Figure 1. The various regions of resistance dominance in the feasible space and the area of infeasible solution as a function of J_e/J_0.

(a) $J_e/J_0 = 0.06$; (b) $J_e/J_0 = 0.12$; (c) $J_e/J_0 = 0.16$; and (d) $J_e/J_0 = 0.2$.

dissolving pectin and sucrose in distilled water of various compositions. The cross-flow velocities were selected such that laminar flow regime was maintained in the filtration chamber during electro-UF. The range of the operating conditions were as follows: feed composition: 1 kg m^{-3} + 14 Brix, 3 kg m^{-3} + 12 Brix, 5 kg m^{-3} + 10 Brix; transmembrane pressure drop: 220, 360, 500, and 635 kPa, cross-flow velocity: 0.09, 0.12, 0.15, and 0.18 m s^{-1}; electric field strength: 0, 300, 600, and 800 V m^{-1}. The term "Brix" represents the strength of aqueous solution of sugar as a percentage by weight (% w/w).

Procedure

Conduction of experiments. During experiment, permeate samples were collected at different time points. The duration of each experiment was 30–40 min. All experiments were conducted at 30°C ± 2°C. Each experiment was repeated three times. All the experiments showed repeatability within ±3% in terms of flux measurement. At the end of each experiment, the membrane was washed in situ thoroughly for 45 min by recirculating distilled water. After that, the cell was emptied and the membrane was removed from the experimental cell and was dipped in hydrochloric acid at pH 3.0 for 45 min. This was followed by washing with distilled water. Thereafter, the membrane was dipped in sodium hydroxide solution at pH 10 for 30 min. Finally, the membrane was repeatedly washed with distilled water. After such thorough washing, water flux was measured with distilled water. This procedure resulted in a recovery of the initial water flux within ±5%.

Analysis of the feed and sample. The concentration of pectin and sucrose in the feed, permeate, and retentate were determined using a Genesys2 Spectrophotometer. For pectin concentration, a wavelength of 230 nm was used, and distilled water was taken as a blank. For pectin–sucrose mixture, the pectin-free solution containing same amount of sucrose was used as a blank. The sucrose content in the sample was assessed with a refractometer (Thermospectronic, USA). Zeta potential of the pectin particle in the feed solutions 1 kg m^{-3} + 14 Brix, 3 kg m^{-3} + 12 Brix, and 5 kg m^{-3} + 10 Brix was measured by Zetasizer (Malvern Zeta Sizernano, USA) and found to be −19.4, −20.5, and −20.1 mV, respectively. All the measurements were made in triplicate, and the averages were taken. The ionic strength of the feed solution did not differ much across the three suspensions, causing no significant change in the zeta potential. In fact, the experimental zeta potential values showed 20 ± 0.6 mV.

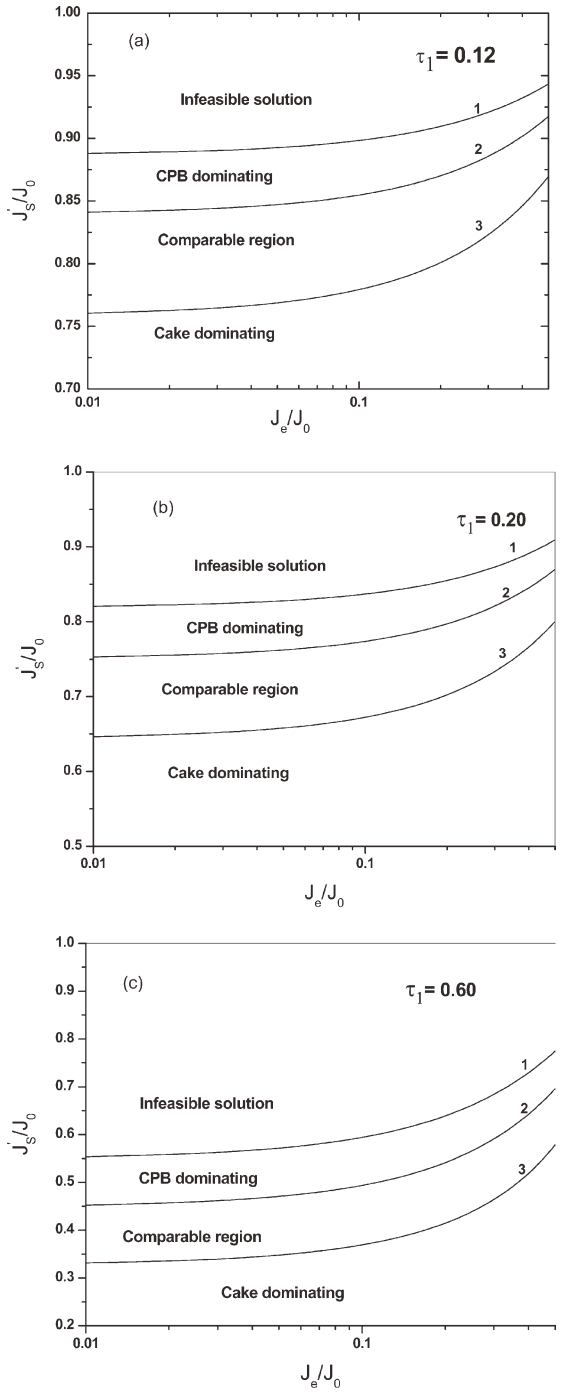

Figure 2. The various regions of resistance dominance in the feasible space and the area of infeasible solution as a function of τ_1.

(a) $\tau_1 = 0.12$; (b) $\tau_1 = 0.20$; and (c) $\tau_1 = 0.60$.

Viscosity of the feed solutions corresponding to the concentration levels stated earlier was measured by Ostwald viscometer and was found to be 1.83×10^{-3}, 2.72×10^{-3}, 3.1×10^{-3} Pa s, respectively. Additional details on the analysis of feed and permeate sample were provided elsewhere.[28]

Results and Discussion

It is evident from the analysis presented in Theory section that $J'_s/J_0 = 0.5$, J'_s/J_0, and τ_1 are three nondimensional parameters that dictate the various fouling zones. The phase-space plots of these parameters are demonstrated in Figures 1a–d to describe the fouling regions, namely, complete pore-blocking dominating region, cake filtration dominating region, and the region where both are equally important.

Figures 1a–d show the boundary of feasible region of various fouling mechanisms in the parameter space. The feasible region is further subdivided into three parts, i.e., complete pore-blocking dominating region, comparable region, and cake dominating region. Curves 1, 2, and 3 are obtained from the characteristic equations 20, 21, and 22, respectively. It can be seen from the figure that any point resulting from arbitrary combination of parameters, which lies on the right side of the Curve 1, leads to infeasible solution zone. In this zone, various combinations of parameters are not allowed; in other words, in this region, solution does not exist. It is interesting to note that it is possible to achieve a very high permeate flux (close to pure water flux) even in the cake dominating region when the value of τ_1 is less than 0.01. It may be observed from the figure that for a fixed value of electric field and transmembrane pressure and for a given membrane, an increase in τ_1 results in the shifting of the fouling regime from cake dominating to complete pore-blocking dominating. Similar trends are observed for different values of J_e/J_0. For example, for a fixed value of $J_e/J_0 = 0.06$ (Figure 1a), when $J'_s/J_0 = 0.5$, the filtration is cake dominating up to $\tau_1 = 0.5$; for the values of τ_1 from 0.5 to 0.75, both the resistances are equally significant and beyond 0.75 up to 1.0, the filtration is complete pore blocking dominating. Further increase in the value of τ_1 (dimensionless characteristic time of complete pore blocking) leads to infeasible solution zone. The effect of electric field on the fouling mechanism is described in Figures 1a–d. It can also be noticed from Figures 1a–d that for a fixed value of transmembrane pressure and for a given membrane, with increasing electric field, i.e., with increasing J_e/J_0, Curves 1, 2, and 3 are shifted toward the right. It appears that with increasing electric field, cake dominating region gets expanded without significant change in width of the comparable and complete pore-blocking region while infeasible region gets reduced. This means that the time required for pore blocking increases with electric field strength. As the electric field strength increases, the particles are lifted from the membrane surface from the start of the operation leading to increase in blocking time.

It is clear that with increasing electric field, both J_e/J_0 and J'_s/J_0 increase. To achieve a constant throughput from a particular membrane at a constant transmembrane pressure, with increasing electric field, fouling mechanism shifts from cake dominating region to complete pore blocking region. For example, for a fixed value of $J'_s/J_0 = 0.6$, with increasing the value of J_e/J_0 from 0.06 to 0.2 (Figures 1a, d), the value of τ_1 increases from 0.25 to 0.3, thereby shifting the fouling mechanism from cake dominating to comparable region. Hence, by manipulating operating conditions, it is possible for an operator to control the membrane fouling during electric field-assisted UF.

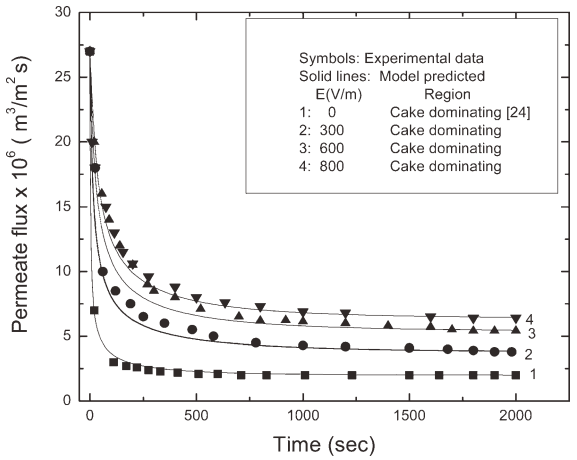

Figure 3. Variation of permeate flux with time for different electric field.

$c_0 = 3$ kg m^{-3} + 12 Brix; $\Delta P = 360$ kPa; $u = 0.12$ m s^{-1}. Curve 1: $E = 0$ V m^{-1}, $k_b = 0.25 \pm 0.02$ s^{-1}, $k_c = (6 \pm 0.5) \times 10^8$ s m^{-2}, $J_s'/J_0 = 0.074$, $J_e/J_0 = 0$, $\tau_1 = 0.25$; Curve 2: $E = 300$ V m^{-1}, $k_b = 0.042 \pm 0.003$ s^{-1}, $k_c = (1.1 \pm 0.1) \times 10^8$ s m^{-2}, $J_s'/J_0 = 0.14$, $J_e/J_0 = 0.06$, $\tau_1 = 0.27$; Curve 3: $E = 600$ V m^{-1}, $k_b = 0.022 \pm 0.001$ s^{-1}, $k_c = (6 \pm 0.5) \times 10^7$ s m^{-2}, $J_s'/J_0 = 0.2$, $J_e/J_0 = 0.12$, $\tau_1 = 0.30$; Curve 4: $E = 800$ V m^{-1}, $k_b = 0.016 \pm 0.001$ s^{-1}, $k_c = (4.5 \pm 0.4) \times 10^7$ s m^{-2}, $J_s'/J_0 = 0.24$, $J_e/J_0 = 0.16$, $\tau_1 = 0.32$.

The fouling mechanism can also be seen in Figures 2a–c for a wide range of electric field. These figures show the phase plot of J_s'/J_0 against J_e/J_0 at different values of τ_1. Curves 1, 2, and 3 are obtained from the characteristic equations 20, 21, and 22, respectively. It can be observed from Figure 1a that for a cake-dominated filtration, one cannot expect a value of J_s'/J_0 more than 0.78 when $J_e/J_0 = 0.1$ and $\tau_1 = 0.12$. However, one can get a higher value of J_s'/J_0 at about 0.86 even under cake-dominated region where $J_e/J_0 = 0.5$. For a value of $J_e/J_0 = 0.1$, one can get a value of J_s'/J_0 in between 0.78 to 0.85, where both cake and complete pore blocking resistances are equally important. One can get even higher value of J_s'/J_0 in between 0.85 to 0.89, where the filtration mechanism is dominated by complete pore blocking. The value of dimensionless characteristic time of complete pore blocking (τ_1) has a strong effect on fouling mechanism. Comparing Figures 2b, c, it can be observed that for a particular membrane and for a fixed value of electric field and transmembrane pressure (for a fixed value of J_e/J_0), with decreasing the value of τ_1 (dimensionless characteristic time of complete pore blocking), fouling mechanism is shifted from complete pore blocking dominating region to cake dominating region. This is because with decreasing τ_1, complete pore blocking resistance decreases while cake resistance increases. For example, at $J_s'/J_0 = 0.55$ and $J_e/J_0 = 0.1$, with decreasing the value of τ_1 from 0.60 to 0.20, fouling mechanism is shifted from complete pore blocking dominating region to cake dominating region.

Figure 3 shows the effect of electric field on the transient behavior of permeate flux for fixed values of feed concentration, cross-flow velocity, and transmembrane pressure. The symbols are the experimental data, and the solid lines are the model predictions. The parameters estimated to various electric fields are shown in Figure 3. From the phase-space plot (Figure 1), one can find that in the presence of electric field, filtration region falls in the cake-dominated region by looking into the values of three parameters (J_s'/J_0, J_e/J_0, and τ_1). The experimental results show the sluggish decline in permeate flux with increasing electric field. This can be explained by the fact that the rate of solute deposition decreases with the increase in electric field. On application of external d.c. electric field with appropriate polarity, the electrophoretic migration of pectin molecules toward the positive electrode causes reduction of net solute flux to the membrane surface. Therefore, both pore blocking and cake layer resistance decrease. This leads to an enhancement of permeate flux. This is evident from the values of the blocking and cake formation coefficients (k_b and k_c). For example, with an increase in electric field from 0 to 800 V m^{-1} for a fixed feed concentration (3 kg m^{-3} + 12 Brix), pressure (360 kPa), and cross-flow velocity (0.12 m s^{-1}), the permeate flux increases by a factor of 3.2. The decrease of k_b is from 0.25 to 0.016 s^{-1} and that for k_c is from 6×10^8 to 4.5×10^7 s m^{-2}.

Figure 4 shows the variation of the resistance ratios with time for different values of k_c. This figure corresponds to data for a fixed feed concentration (3 kg m^{-3} + 12 Brix), pressure (360 kPa), cross-flow velocity (0.12 m s^{-1}), and electric field (800 V m^{-1}). In this figure, the value of k_b is kept constant at 0.016 s^{-1} so that the sensitivity of the k_c can be realized in terms of fouling mechanism. According to phase-space plot, Figure 1c, one can see that curves 1, 2, 3, and 4 lie in the domain of cake dominating, comparable region, at the boundary of comparable and complete pore blocking region and complete pore blocking region, respectively. The figure clearly shows that τ_1 is exclusively influenced by k_c. For example, when k_c changes from $(4.5 \pm 0.5) \times 10^7$ to $(6.7 \pm 0.5) \times 10^8$ s m^{-2}, τ_1 increases from 0.32 to 1.79 keeping other parameters unchanged. This indicates that with increasing k_c, the onset of cake formation is delayed

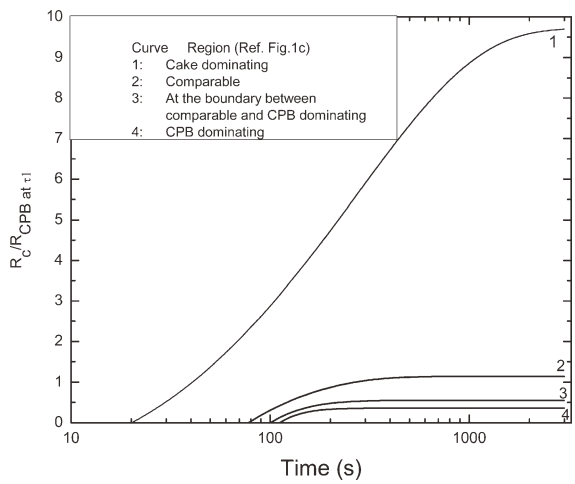

Figure 4. Value of the ratio of R_c/R_{CPB} at τ_1 is plotted for different values of k_c.

$E = 800$ V m^{-1}; $c_0 = 3$ kg m^{-3} + 12 Brix; $u = 0.12$ m s^{-1}; $\Delta P = 360$ kPa; $k_b = 0.016$ s^{-1}; $J_s'/J_0 = 0.24$; $J_e/J_0 = 0.16$. Curve 1: $k_c = (4.5 \pm 0.5) \times 10^7$ s m^{-2}, $\tau_1 = 0.32$; Curve 2: $k_c = (2.25 \pm 0.3) \times 10^8$ s m^{-2}, $\tau_1 = 1.245$; Curve 3: $k_c = (4.5 \pm 0.4) \times 10^8$ s m^{-2}, $\tau_1 = 1.61$; Curve 4: $k_c = (6.7 \pm 0.5) \times 10^8$ s m^{-2}, $\tau_1 = 1.79$.

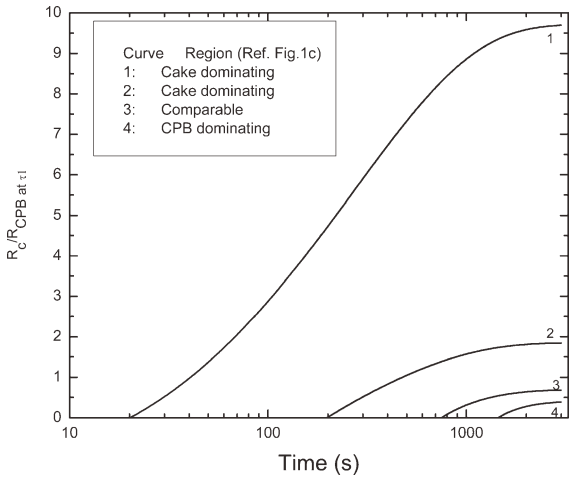

Figure 5. Value of the ratio of R_c/R_{CPB} at τ_1 is plotted for different values of k_b.

$E = 800$ V m^{-1}; $c_0 = 3$ kg m^{-3} + 12 Brix; $u = 0.12$ m s^{-1}; $\Delta P = 360$ kPa; $k_c = (4.5 \pm 0.5) \times 10^7$ s m^{-2}; $J_s'/J_0 = 0.24$; $J_e/J_0 = 0.16$. Curve 1: $k_b = 16 \times 10^{-3}$ s^{-1}, $\tau_1 = 0.32$; Curve 2: $k_b = 5 \times 10^{-3}$ s^{-1}, $\tau_1 = 0.99$; Curve 3: $k_b = 2 \times 10^{-3}$ s^{-1}, $\tau_1 = 1.5$; Curve 4: $k_b = 1.2 \times 10^{-3}$ s^{-1}, $\tau_1 = 1.74$.

resulting in shifting of fouling mechanism from cake dominating to complete pore blocking. This is consistent with the results reported by Mondal and De[24] in case of zero electric field. This also corresponds to an increase in complete pore-blocking resistance (R_{CPB}). At constant J_s', the total resistance is fixed. Therefore, comparing Curves 1 and 4, an increase in k_c from $(4.5 \pm 0.5) \times 10^7$ to $(6.7 \pm 0.5) \times 10^8$ s m^{-2} results in a decrease in R_c/R_{CPB} from 9.69 to 0.359 at steady state.

Figure 5 illustrates the variation of the resistance ratios with time for different values of k_b. This figure corresponds to data for a fixed feed concentration (3 kg m^{-3} + 12 Brix), pressure (360 kPa), cross-flow velocity (0.12 m s^{-1}), and electric field (800 V m^{-1}). In this figure, the value of k_c is kept constant at $(4.5 \pm 0.4) \times 10^7$ s m^{-2} so that the sensitivity of the k_b can be realized in terms of fouling phenomena. According to the phase-space plot (Figure 1c), one can see that Curves 1 and 2 lie in the domain of cake dominating, whereas Curves 3 and 4 fall in the domain of comparable region and complete pore blocking region, respectively. It is evident from the figure that with decreasing k_b from 16×10^{-3} to 1.2×10^{-3} s^{-1}, τ_1 increases from 0.32 to 1.74, resulting in shifting of fouling mechanism from cake dominating region to complete pore blocking region keeping other parameters unaltered. This indicates that the onset of cake formation is delayed by decreasing k_b for a fixed steady-state flux. Similar observations were reported by Mondal and De[24] in case of zero electric field.

Figure 6 describes the permeate flux profile for different feed solute concentrations for fixed values of electric field, cross-flow velocity, and transmembrane pressure. The symbols are the experimental data, and the solid lines are the model predictions. The model parameters estimated corresponding to Curves 1, 2, and 3 are shown in Figure 6. A close look into the values of three nondimensional parameters (J_s'/J_0, J_e/J_0, and τ_1) indicates that the filtration shown in Figure 6 is cake dominating according to the phase-space plot (Figures 1c, d and 2b). The sharp decline in permeate flux observed at the beginning of filtration can be attributed to the rapid pore blocking of pectin molecules on the membrane and to the increase in concentration polarization. As the time of operation progresses, there is more accumulation of solutes over the membrane surface leading to severe concentration polarization. The slower flux decline at later stages can be attributed to the formation of cake layer on the membrane surface. It is further noticed that an increase in flux is observed with decrease in feed concentration keeping other operating conditions unchanged. With increase in solute feed concentration, concentration polarization increases resulting in an increase in cake layer thickness over the membrane surface. This leads to decrease in permeate flux with increase in both k_b and k_c. For example, with an increase in feed concentration from 1 kg m^{-3} + 14 Brix to 5 kg m^{-3} + 10 Brix for a fixed electric field (800 V m^{-1}), pressure (360 kPa), and cross-flow velocity (0.12 m s^{-1}), the steady-state permeate flux decreases from 9.1 to 5.2 m^3 m^{-2} s^{-1}. Increase in the value of k_b is from 0.012 to 0.022 s^{-1} and that for k_c is from 4.0×10^7 to 6.0×10^7 s m^{-2}, respectively.

Figure 7 presents the transient behavior of permeate flux at different operating pressure differences for fixed values of feed concentration, electric field, and cross-flow velocity. The symbols are the experimental data, and the solid lines are the model predictions. The parameters calculated corresponding to Curves 1, 2, and 3 in Figure 7 indicate that the filtration is cake dominating according to the phase-space plot (Figures 1c, b and 2a). It may be mentioned that the transmembrane pressure drop affects the cake compressibility directly. Cake compressibility appears in the definition of cake resistance, $R_c = \alpha(1 - \varepsilon_c)\, \rho_c\, L$, where α is the specific cake resistance, ε_c is cake porosity, ρ_c is the cake density, and L is the cake layer thickness. Of these parameters, specific cake resistance is a function of transmembrane pressure

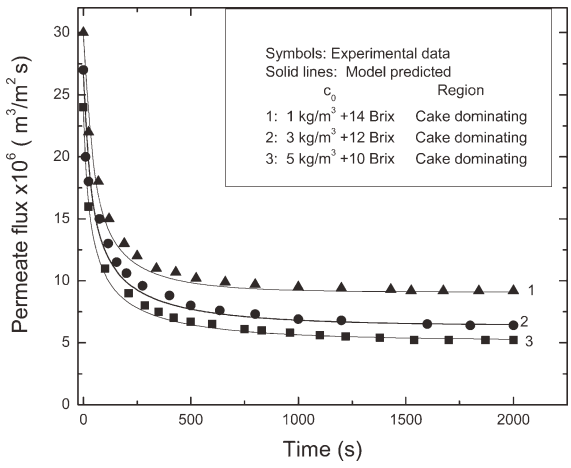

Figure 6. Variation of permeate flux with time at deferent feed concentration.

$\Delta P = 360$ kPa; $E = 800$ V m^{-1}; $u = 0.12$ m s^{-1}. Curve 1: $c_0 = 1$ kg m^{-3} + 14 Brix, $k_b = 0.012 \pm 0.001$ s^{-1}, $k_c = (4 \pm 0.4) \times 10^7$ s m^{-2}, $J_s'/J_0 = 0.3$, $J_e/J_0 = 0.2$, $\tau_1 = 0.5$; Curve 2: $c_0 = 3$ kg m^{-3} + 12 Brix, $k_b = 0.016 \pm 0.001$ s^{-1}, $k_c = (4.5 \pm 0.4) \times 10^7$ s m^{-2}, $J_s'/J_0 = 0.24$, $J_e/J_0 = 0.16$, $\tau_1 = 0.325$; Curve 3: $c_0 = 5$ kg m^{-3} + 10 Brix, $k_b = 0.022 \pm 0.002$ s^{-1}, $k_c = (6 \pm 0.5) \times 10^7$ s m^{-2}, $J_s'/J_0 = 0.22$, $J_e/J_0 = 0.15$, $\tau_1 = 0.20$.

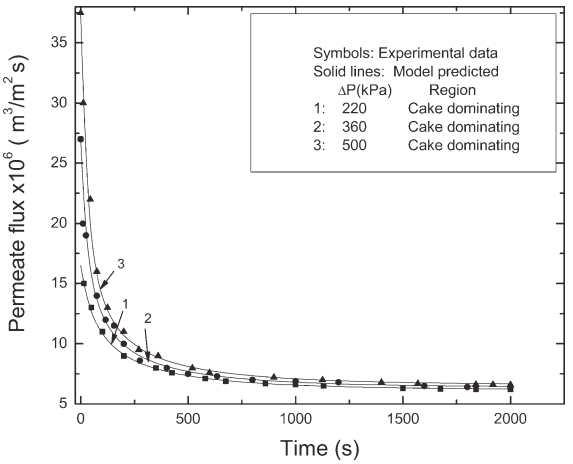

Figure 7. Variation of permeate flux with time at different pressure.

$c_0 = 3$ kg m^{-3} + 12 Brix; $E = 800$ V m^{-1}; $u = 0.12$ m s^{-1}. Curve 1: $\Delta P = 220$ kPa, $k_b = 0.008 \pm 0.0004$ s^{-1}, $k_c = (4.8 \pm 0.5) \times 10^7$ s m^{-2}, $J_s'/J_0 = 0.38$, $J_e/J_0 = 0.25$, $\tau_1 = 0.12$; Curve 2: $\Delta P = 360$ kPa, $k_b = 0.016 \pm 0.001$ s^{-1}, $k_c = (4.5 \pm 0.4) \times 10^7$ s m^{-2}, $J_s'/J_0 = 0.24$, $J_e/J_0 = 0.16$, $\tau_1 = 0.325$; Curve 3: $\Delta P = 500$ kPa, $k_b = 0.017 \pm 0.001$ s^{-1}, $k_c = (4 \pm 0.4) \times 10^7$ s m^{-2}, $J_s'/J_0 = 0.18$, $J_e/J_0 = 0.12$, $\tau_1 = 0.60$.

drop as $\alpha = \alpha_0 (\Delta P)^n$, where n and α_0 are the cake compressibility index and coefficient, respectively. For compressible cake, n is less than 1 and it is 1 for incompressible cake layer. It is well known that the steady-state flux in cake governing filtration is a weak function of ΔP at lower operating pressure range and is independent at higher operating pressure. This is true for pectin solution.[33] In such cases, the cake resistance and, consequently, the parameter values vary accordingly. As shown in Figure 7, as ΔP increases, the values of k_c vary weakly from 4.8×10^7 to 4×10^7 s m^{-2}. On the other hand, variation of k_b is significant when ΔP increases from 220 to 360 kPa, i.e., from 0.008 to 0.016 s^{-1}. This implies that duration of pore blocking increases from 15 to 20 s. At higher range of ΔP, as steady-state flux is independent of ΔP, values of k_b at 360 and 500 kPa are invariant, but the duration of pore blocking increases from 20 to 35 s. Hence, at lower range of ΔP, as the compressibility of cake increases, duration of the pore blocking increases associated with an increase in blocking coefficient. As the cake becomes incompressible, the blocking coefficient remains almost invariant, but the duration of blocking increases. Thus, with increase in ΔP, more solutes are convected toward the membrane surface, increasing the blocking duration. This explains the trend of experimental results that at the early stage of the experiment, permeate flux declines more rapidly with increasing transmembrane pressure. Moreover, the effect of the increased pressure on the steady-state permeate flux is not significant at higher applied pressures because effects of pressure is marginal on steady-state flux in a cake-controlling case.

Figure 8 presents the effect of cross-flow velocity (or shear rate) on the decline in permeate flux for fixed values of feed concentration, electric field, and transmembrane pressure. The symbols are the experimental data, and the solid lines are the model predictions. The estimated model parameter corresponding to Curves 1 and 2 in Figure 8 indicate that the filtration is cake dominating according to the phase-space plot (Figure 1). It can also be seen that increasing cross-flow velocity has a strong effect on the model parameters. From the results shown in this figure, it is clear that for a fixed electric field, with increase in cross-flow velocity, permeate flux increases and both pore blocking and cake resistance coefficients decrease. At higher cross-flow velocity, cake layer thickness on the membrane surface is lower due to forced convection. This behavior is a direct result of enhancement of turbulence in the flow channel that increases the rate of transfer of solute particles from the membrane surface to the bulk flow resulting in decrease in concentration polarization near the membrane surface. This restricts the formation and growth of cake layer on the membrane surface, leading to an increase in permeate flux. Furthermore, with increasing cross-flow velocity (shear rate), the retained solute particles tend to block the membrane pores at a slower rate. Therefore, both complete pore blocking constant (k_b) and cake filtration constant (k_c) show a decreasing trend with increasing cross-flow velocity. For example, at 800 V m^{-1}, pressure of 360 kPa, and a feed concentration of 3 kg m^{-3} + 12 Brix, with increase in cross-flow velocity from 0.09 to 0.12 m s^{-1}, k_b and k_c decrease from 0.024 to 0.01 s^{-1} and from 6.0×10^7 to 3.5×10^7 s m^{-2}, respectively. This results in an augmentation of permeate flux from 6.3 to 6.9 m^3 m^{-2} s^{-1}.

Figure 9 demonstrates the growth of cake layer resistance at different electric field values. From the figure, it is evident that cake layer resistance decreases with increase in electric field. Applied electric field reduces the cake layer resistance due to electrophoretic migration of the pectin molecules away from the membrane surface, i.e., opposite of the convective flow of permeate, resulting to decrease in cake layer thickness. It should be noted that according to the phase-space plot (Figure 1), this figure corresponds to cake-dominated region. It can also be observed that increasing electric

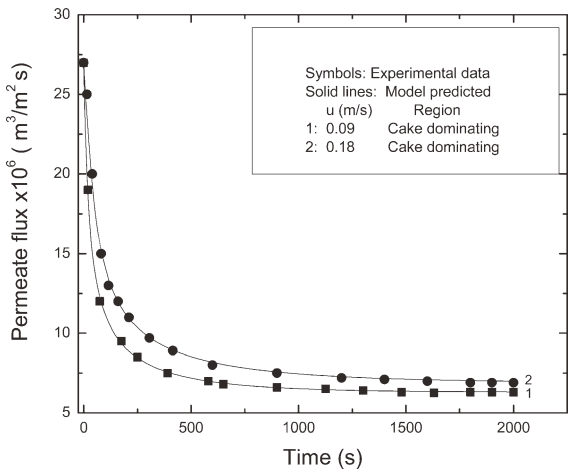

Figure 8. Variation of permeate flux with time at different cross-flow velocity.

$c_0 = 3$ kg m^{-3} + 12 Brix; $E = 800$ V m^{-1}; $\Delta P = 360$ kPa. Curve 1: $u = 0.09$ m s^{-1}, $k_b = 0.024 \pm 0.003$ s^{-1}, $k_c = (6.0 \pm 0.5) \times 10^7$ s m^{-2}, $J_s'/J_0 = 0.23$, $J_e/J_0 = 0.16$, $\tau_1 = 0.26$; Curve 2: $u = 0.18$ m s^{-1}, $k_b = 0.01 \pm 0.001$ s^{-1}, $k_c = (3.5 \pm 0.3) \times 10^7$ s m^{-2}, $J_s'/J_0 = 0.25$, $J_e/J_0 = 0.16$, $\tau_1 = 0.42$.

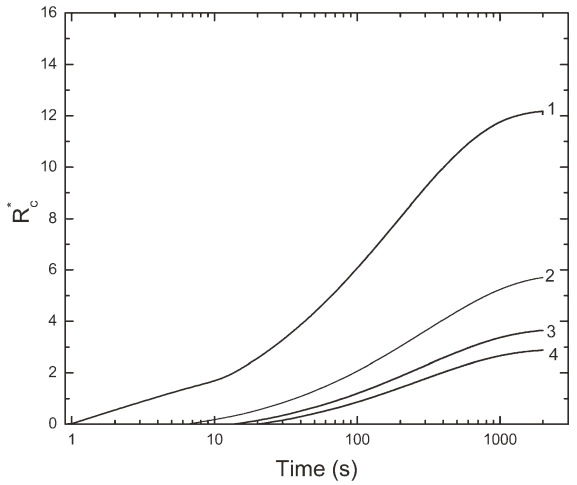

Figure 9. Variation of cake layer resistance with time at different electric field.

$c_0 = 3$ kg m^{-3} + 12 Brix; $\Delta P = 360$ kPa; $u = 0.12$ m s^{-1}. Curve 1: $E = 0$ V m^{-1}, $\tau_1 = 0.25$, $t_1 = 1.04$ s, $J_s'/J_0 = 0.074$, $J_e/J_0 = 0$, $R^*_{CPB} = 0.28$; Curve 2: $E = 300$ V m^{-1}, $\tau_1 = 0.27$, $t_1 = 6.5$ s, $J_s'/J_0 = 0.14$, $J_e/J_0 = 0.06$, $R^*_{CPB} = 0.29$; Curve 3: $E = 600$ V m^{-1}, $\tau_1 = 0.30$, $t_1 = 13.65$ s, $J_s'/J_0 = 0.2$, $J_e/J_0 = 0.12$, $R^*_{CPB} = 0.30$; Curve 4: $E = 800$ V m^{-1}, $\tau_1 = 0.32$, $t_1 = 20.25$ s, $J_s'/J_0 = 0.24$, $J_e/J_0 = 0.16$, $R^*_{CPB} = 0.30$.

field delays the onset of cake formation, indicated by a higher value of transition time. Therefore, by increasing electric field, one can reduce the cake thickness and can operate at higher steady-state flux. For example, at 800 V m^{-1}, transition time increases from 1.04 to 20.25 s, and nondimensional steady-state cake resistance increases from 2.87 to 12.2 when compared with zero electric field.

The profiles of cake resistance with time at various feed concentration for a fixed value of electric field, transmembrane pressure, and cross-flow velocity are shown in Figure 10. From Figures 1d, c and 2b, it should be noted that filtrations shown in this figure are cake dominating. It is evident from the figure that cake layer resistance increases with increase in feed concentration at a particular time of operation. The concentration polarization increases with increase in feed concentration, resulting in higher cake layer thickness and thereby, increasing the value of cake layer resistance. As observed from the figure, with increase in feed concentration, the time for the onset of cake formation decreases. This is because of deposition of thicker cake layer at higher feed concentrations. For example, with an increase in feed concentration from 1 kg m^{-3} + 14 Brix to 5 kg m^{-3} + 10 Brix, for a fixed electric field (800 V m^{-1}), transmembrane pressure drop (360 kPa), and cross-flow velocity (0.12 m s^{-1}), the time required for the onset of cake formation decreases from 41.85 to 8.8 s and the nondimensional steady-state cake resistance increases from 1.83 to 3.37.

Figure 11 represents a plot for the variation of cake layer thickness with time for different values of cross-flow velocities. From Figure 1c, it should be noted that filtrations shown in this figure are cake dominating. It may be observed from the figure that cake layer resistance decreases with increase in cross-flow velocity. This is simply because at higher cross-flow velocity, the cake layer thickness is less due to the forced convection imparted by the higher cross-flow velocity. This effect of cross-flow velocity on the transition time from complete pore blocking to cake formation is also noticed. Keeping other operating conditions unaltered, increasing cross-flow velocity delays the transition for onset of cake formation. For example, at electric field (800 V m^{-1}), pressure (360 kPa), feed concentration (3 kg m^{-3} + 12 Brix), with increase in cross-flow velocity from 0.09 to 0.18 m s^{-1}, the transition time increases from 11.0 to 42.0 s and the nondimensional steady-state cake resistance decreases from 3.0 to 2.45.

Conclusions

Membrane fouling during electric field-assisted UF of synthetic juice (a mixture of pectin and sucrose) consists of complete pore blocking followed by cake formation, in sequence, resulting to an initial rapid flux decline followed by gradual flux decline. The initial rapid flux decline is due to complete pore blocking by pectin molecules while the cake formation over the membrane surface is responsible for gradual flux decline. Experimental results revealed that the flux decline is controlled by cake formation mechanism for all the experimental conditions studied herein. However, this model is also useful to explain the transient behavior of permeate flux during complete pore blocking dominating electric field-assisted UF as well as when both cake formation and complete pore blocking become equally dominant. Filtration mechanism is likely to be dominated by either of these mechanisms under favorable operating conditions (i.e., low feed concentration, low pressure, high electric field, and high cross-flow velocity) when the accumulation of the solutes near the membrane surface is low. Regarding the experimental validation of these cases, it may be mentioned that the experimental data available typically belong to the cake dominating regime. The present model quantitatively

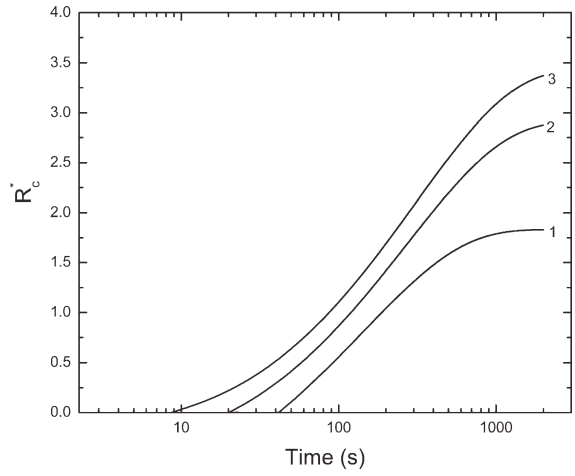

Figure 10. Variation of cake layer resistance with time at different feed concentration.

$\Delta P = 360$ kPa; $E = 800$ V m^{-1}; $u = 0.12$ m s^{-1}. Curve 1: $c_0 = 1$ kg m^{-3} + 14 Brix, $\tau_1 = 0.5$, $t_1 = 41.85$ s, $J_s'/J_0 = 0.3$, $J_e/J_0 = 0.2$, $R^*_{CPB} = 0.46$; Curve 2: $c_0 = 3$ kg m^{-3} + 12 Brix, $\tau_1 = 0.32$, $t_1 = 20.25$ s, $J_s'/J_0 = 0.24$, $J_e/J_0 = 0.16$, $R^*_{CPB} = 0.30$; Curve 3: $c_0 = 5$ kg m^{-3} + 10 Brix, $\tau_1 = 0.2$, $t_1 = 8.8$ s, $J_s'/J_0 = 0.22$, $J_e/J_0 = 0.15$, $R^*_{CPB} = 0.17$.

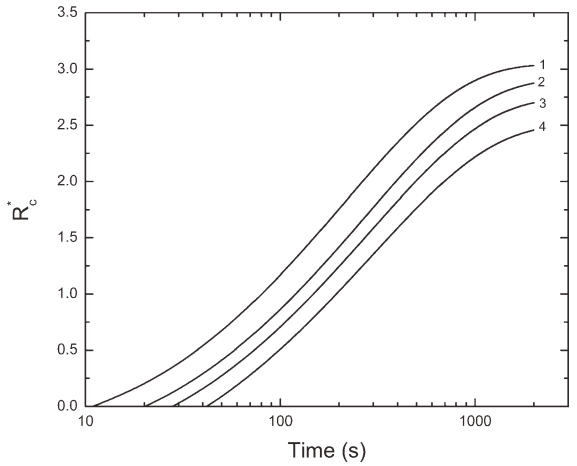

Figure 11. Variation of cake layer resistance with time at different cross-flow velocity.

c_0 = 3 kg m^{-3} + 12 Brix; E = 800 V m^{-1}; ΔP = 360 kPa; J_e/J_0 = 0.16. Curve 1: u = 0.09 m s^{-1}, τ_1 = 0.26, t_1 = 11.0 s, J_s'/J_0 = 0.23, R^*_{CPB} = 0.24; Curve 2: u = 0.12 m s^{-1}, τ_1 = 0.32, t_1 = 20.25 s, J_s'/J_0 = 0.24, R^*_{CPB} = 0.3; Curve 3: u = 0.15 m s^{-1}, τ_1 = 0.36, t_1 = 28.0 s, J_s'/J_0 = 0.244, R^*_{CPB} = 0.35; Curve 4: u = 0.18 m s^{-1}, τ_1 = 0.42, t_1 = 42.0 s, J_s'/J_0 = 0.25, R^*_{CPB} = 0.40.

describes the influence of operating conditions such as electric field, feed concentration, and cross-flow velocity on the transition of fouling mechanism from complete pore blocking to cake formation. Experimental observations confirm that the time required for the onset of cake formation increases with increase in electric field, cross-flow velocity, pressure, and decrease in feed concentration. For example, at 800 V m^{-1}, the transition time from complete pore blocking to cake formation increases from 1.04 to 20.25 s when compared with zero electric field. The present model is shown to be in good agreement with the experimental flux data, with the model parameters identifying the fouling mechanism during electric field-assisted UF of synthetic juice. Moreover, this model should be of immense help for designing electro-UF unit for the separation of cake forming charged solute.

Notation

a_1, a_2, a_3, A_3 = coefficients defined in Eq. 16
A_1, A_4 = coefficients defined in Eq. 4
c_0 = pectin concentration at bulk, kg m^{-3}
D_i = dielectric constant, dimensionless
E = electric field, V m^{-1}
J = permeate flux, m^3 m^{-2} s^{-1}
J_0 = permeate flux at t = 0, m^3 m^{-2} s^{-1}
J_s = steady-state permeate flux at zero electric field, m^3 m^{-2} s^{-1}
J_e = electrophoretic velocity, m s^{-1}
J_s' = steady-state permeate flux in the presence of electric field, m^3 m^{-2} s^{-1}
J_{t_1} = permeate flux at time $t = t_1$, m^3 m^{-2} s^{-1}
$J_{i,exp}$ = experimental permeate flux at ith time point, m^3 m^{-2} s^{-1}
$J_{i,cal}$ = calculated permeate flux at ith time point, m^3 m^{-2} s^{-1}
k_b = complete pore-blocking constant, s^{-1}
k_c = cake filtration constant, s m^{-2}
L = cake layer thickness, m
n = cake compressibility index, dimensionless
Q = coefficients defined in Eq. 17
R_m = hydraulic membrane resistance, m^{-1}
R = coefficients defined in Eq. 17
R_{CPB} = complete pore-blocking resistance, m^{-1}
R^*_{CPB} = nondimensional complete pore-blocking resistance defined as $R^*_{CPB} = \frac{R_{CPB}}{R_m}$
R_c = cake resistance, m^{-1}
R^*_c = nondimensional cake resistance defined as $R^*_c = \frac{R_c}{R_m}$
R^{**}_c = nondimensional cake resistance defined as $R^{**}_c = \frac{R^*_c}{1+R^*_{CPB}}$
R^*_{cs} = nondimensional steady-state cake resistance defined as $R^*_{cs} = \frac{R_{cs}}{R_m}$
R^*_{cs} = nondimensional steady-state cake resistance defined as $R^{**}_{cs} = \frac{R^*_{cs}}{1+R^*_{CPB}}$
t = time, s
t_1 = transition time from complete pore blocking to onset of cake formation, s
u = average bulk velocity, m s^{-1}

Greek letters

τ = characteristic time constant defined as $\tau = k_b t$
α = specific cake resistance, m kg^{-1}
α_0 = coefficient, m kg^{-1}
ε_c = cake porosity, dimensionless
ρ_c = cake density, kg m^{-3}
μ = viscosity of permeate, Pa s
η = viscosity of feed solution, Pa s
ζ = zeta potential of particle, V
ε_o = permittivity of vacuum (8.854 $\times$ 10^{-12}), CV^{-1} m^{-1}
ΔP = transmembrane pressure difference, Pa
θ = defined in Eq. 17

Literature Cited

1. Todisco S, Pena L, Drioli E, Tallarico P. Analysis of the fouling mechanism in microfiltration of orange juice. *J Food Process Preservation*. 1996;20:453–466.
2. Capannelli G, Bottino A, Munari S. The use of membrane processes in the clarification of orange and lemon juices. *J Food Eng*. 1994;21:473–483.
3. Jiraratananon R, Uttapap D, Tangamornsuksun C. Self forming dynamic membrane for ultrafiltration of pineapple juice. *J Membr Sci*. 1997;129:135–143.
4. Blatt WF, Dravid A, Michaeles AS, Nelson L. Solute polarization and cake formation in membrane ultrafiltration: causes, consequences and control techniques. In: Flinn JE, editor. *Membrane Science and Technology*. New York: Plenum Press, 1970: 47–97.
5. Yu ZR, Chiang BH, Hwang LS. Retention of passion fruit juice compounds by ultrafiltration. *J Food Sci*. 1986;51:841–844.
6. De S, Bhattacharjee S, Sharma A, Bhattacharya PK. Generalized integral and similarity solution of the concentration profiles for osmotic pressure controlled ultrafiltration. *J Membr Sci*. 1997; 130:99–121.
7. De S, Bhattacharya PK. Modelling of ultrafiltration process for a two component aqueous solution of low and high (gel forming) molecular weight solutes. *J Membr Sci*. 1997;136:57–69.
8. Karode SK. A method for prediction of the gel layer concentration in macromolecule ultrafiltration. *J Membr Sci*. 2000;171:131–139.
9. Hérmia J. Constant pressure blocking filtration laws. Applications to power-law non-Newtonian fluids. *Trans IChemE*. 1982;60:183–187.
10. Field RW, Wu D, Howell JA, Gupta BB. Critical flux concept for microfiltration fouling. *J Membr Sci*. 1995;100:250–272.
11. Hermans PH, Bredee HL. Principles of the mathematical treatment of constant-pressure filtration. *J Soc Chem Ind*. 1936;55T:1–11.
12. Hwang KJ, Liao CY, Tung KL. Analysis of particle fouling during microfiltration by use of blocking models. *J Membr Sci*. 2007;287:287–293.
13. Yuan W, Kocic A, Zydney AL. Analysis of humic acid fouling during microfilake filtration model. *J Membr Sci*. 2002;198:51–62.
14. Vincent-Vela MC, Alvarez-Blanco S, Lora-Garcia J, Bergantinos-Rodriguez E. Analysis of membrane pore blocking models

applied to the ultrafiltration of PEG. *Sep Purif Technol*. 2008;62: 489–498.
15. Purkait MK, Bhattachaya PK, De S. Membrane filtration of leather plant effluent: flux decline mechanism. *J Membr Sci*. 2005;258: 85–96.
16. Bowen WR, Gan Q. Properties of microfiltration membranes: flux loss during constant pressure permeation of bovine serum albumin. *Biotechnol Bioeng*. 1991;38:688–696.
17. Ho CC, Zydney AL. A combined pore blockage and cake filtration model for protein fouling during microfiltration. *J Colloid Interface Sci*. 2000;232:389–399.
18. Jonsson G, Prádanos P, Hernández A. Fouling phenomena in microporous membranes. Flux decline kinetics and structural modifications. *J Membr Sci*. 1996;112:171–183.
19. Lim AL, Bai R. Membrane fouling and cleaning in microfiltration of activated sludge wastewater. *J Membr Sci*. 2003;216:279–290.
20. Jiraratananon R, Uttapap D, Sampranpiboon E. Crossflow microfiltration of a colloidal suspension with the presence of macromolecules. *J Membr Sci*. 1998;140:57–66.
21. Giorno L, Todisco S, Donato LED, Drioli E. Study of fouling phenomena in apple juice clarification by enzyme membrane reactor. *Sep Sci Technol*. 1998;33:739–756.
22. Barros STD, Andrade CMG, Mendes ES, Peres L. Study of fouling mechanism in pineapple juice clarification by ultrafiltration. *J Membr Sci*. 2003;215:213–224.
23. Rai P, Majumdar GC, Sharma G, DasGupta S, De S. Effect of various cutoff membranes on permeate flux and quality during filtration of mosambi (*Citrus sinensis* (L.) Osbeck) juice. *Food Bioproducts Process*. 2006;84:213–219.
24. Mondal S, De S. Generalized criteria for identification of fouling mechanism under steady state membrane filtration. *J Membr Sci*. 2009;344:6–13.
25. Hofmann R, Posten C. Improvement of dead-end filtration of biopolymers with pressure electrofiltration. *Chem Eng Sci*. 2003;58: 3847–3858.
26. Enevoldsen AD, Hansen EB, Jonsson G. Electro-ultrafiltration of industrial enzyme solution. *J Membr Sci*. 2007;299:28–37.
27. Iritani E, Mukai Y, Kiyotomo Y. Effects of electric field on dynamic behaviors of dead-end inclined and downward ultrafiltration of protein solutions. *J Membr Sci*. 2000;164:51–57.
28. Sarkar B, DasGupta S, De S. Effect of electric field during gel-layer controlled ultrafiltration of synthetic and fruit juice. *J Membr Sci*. 2008;307:268–276.
29. Sarkar B, Pal S, Ghosh TB, De S, DasGupta S. A study of electric field enhanced ultrafiltration of synthetic fruit juice and optical quantification of gel deposition. *J Membr Sci*. 2008;311:112–120.
30. Sarkar B, DasGupta S, De S. Flux decline during electric field assisted cross flow ultrafiltration of mosambi (*Citrus sinensis* (L.) Osbeck) juice. *J Membr Sci*. 2009;331:75–83.
31. Hunter RJ. *Zeta Potential in Colloid Science: Principles and Applications*. London: Academic Press, 1981.
32. Spiegel MR, Liu J. *Schaum's Outlines: Mathematical Handbook of Formulas and Tables*. Singapore: McGraw-Hill, 1999.
33. Rai P, Majumdar GC, DasGupta S, De S. Modeling of permeate flux decline of synthetic fruit juice and mosambi juice (*Citrus sinensis* (L.) Osbeck) in stirred continuous ultrafiltration. *LWT Food Sci Technol*. 2007;40:1765–1773.

Manuscript received Sept. 11, 2010, and revision received Apr. 22, 2011.